Hadron spectrum, quark masses, and decay constants from light overlap fermions on large lattices

D. Galletly,[1] M. Gürtler,[2] R. Horsley,[1] H. Perlt,[3] P. E. L. Rakow,[4] G. Schierholz,[2,5] A. Schiller,[3] and T. Streuer[6]

(QCDSF-UKQCD Collaboration)

[1]*School of Physics, University of Edinburgh, Edinburgh EH9 3JZ, United Kingdom*
[2]*John von Neumann-Institut für Computing NIC, Deutsches Elektronen-Synchrotron DESY, D-15738 Zeuthen, Germany*
[3]*Institut für Theoretische Physik, Universität Leipzig, D-04109 Leipzig, Germany*
[4]*Theoretical Physics Division, Department of Mathematical Sciences, University of Liverpool, Liverpool L69 3BX, United Kingdom*
[5]*Deutsches Elektronen-Synchrotron DESY, D-22603 Hamburg, Germany*
[6]*Department of Physics and Astronomy, University of Kentucky, Lexington, Kentucky 40506, USA*
(Received 14 September 2006; revised manuscript received 11 January 2007; published 20 April 2007)

We present results from a simulation of quenched overlap fermions with Lüscher-Weisz gauge field action on lattices up to $24^3 48$ and for pion masses down to ≈ 250 MeV. Among the quantities we study are the pion, rho, and nucleon masses; the light and strange quark masses; and the pion decay constant. The renormalization of the scalar and axial vector currents is done nonperturbatively in the RI-MOM scheme. The simulations are performed at two different lattice spacings, $a \approx 0.1$ fm and ≈ 0.15 fm, and on two different physical volumes, to test the scaling properties of our action and to study finite volume effects. We compare our results with the predictions of chiral perturbation theory and compute several of its low-energy constants. The pion mass is computed in sectors of fixed topology as well.

DOI: 10.1103/PhysRevD.75.073015 PACS numbers: 12.15.Ff, 12.38.Gc, 14.65.Bt

I. INTRODUCTION

Lattice simulations of QCD at small quark masses require a fermion action with good chiral properties. Overlap fermions [1] possess an exact chiral symmetry on the lattice [2], and thus are well suited for this task. Furthermore, overlap fermions are automatically $O(a)$ improved if employed properly [3].

Previous calculations of hadron observables from quenched overlap fermions have been limited to larger quark masses and/or coarser lattices due to the high cost of the simulations [4–7]. To ensure that the correlation functions this involves are not overshadowed by the exponential decay of the overlap operator [8], the lattice spacing a should be small enough such that $m_H a \ll 2$ for mesons and $m_H a \ll 3$ for baryons, where m_H is the mass of the hadron. In addition, the spatial extent of the lattice L should satisfy $L \gg 1/(2f_\pi)$ in order to be able to make contact with chiral perturbation theory [9].

Over the past years we have done extensive simulations of quenched overlap fermions [6,10,11]. Furthermore, we have employed overlap fermions to probe the topological structure of the QCD vacuum at zero [12] and at finite temperature [13]. In this paper we shall give the technical details of our calculations and present results on hadron and quark masses and the pseudoscalar decay constant, including nonperturbative renormalization of the scalar, pseudoscalar, and axial vector currents. The bulk of the simulations are done on the $24^3 48$ lattice at lattice spacing $a \approx 0.1$ fm. Our results on the spectral properties of the overlap operator [6] and nucleon structure functions [10] will be reported elsewhere in detail.

The paper is organized as follows. In Sec. II we discuss the action and how it is implemented numerically. In Sec. III we give the parameters of the simulation. In Sec. IV we present our results for the hadron masses and the pseudoscalar decay constant. The latter is used to set the scale. We compare our results with the predictions of chiral perturbation theory, and attempt to compute some of its low-energy constants. In Sec. V we compute the renormalization constants of the scalar and pseudoscalar densities, as well as the axial vector current, nonperturbatively, and in Sec. VI we present our results for the light and strange quark masses. Finally, in Sec. VII we conclude.

II. THE ACTION

The massive overlap operator is defined by

$$D = \left(1 - \frac{am_q}{2\rho}\right) D_N + m_q \tag{1}$$

with the Neuberger-Dirac operator D_N given by

$$D_N = \frac{\rho}{a}\left(1 + \frac{D_W(\rho)}{\sqrt{D_W^\dagger(\rho) D_W(\rho)}}\right), \qquad D_W(\rho) = D_W - \frac{\rho}{a}, \tag{2}$$

where D_W is the massless Wilson-Dirac operator with $r = 1$, and $\rho \in [0, 2]$ is a (negative) mass parameter. The operator D_N has $n_- + n_+$ exact zero modes, $D_N \psi_n^0 = 0$

 © 2007 The American Physical Society

with $n = 1, \ldots, n_- + n_+$, where n_- (n_+) denotes the number of modes with negative (positive) chirality, $\gamma_5\psi_n^0 = -\psi_n^0$ ($\gamma_5\psi_n^0 = +\psi_n^0$). The index of D_N is thus given by $\nu = n_- - n_+$. The "continuous" modes λ_i, $D_N\psi_i = \lambda_i\psi_i$, satisfy $(\psi_i^\dagger, \gamma_5\psi_i) = 0$ and come in complex conjugate pairs λ_i, λ_i^*.

To evaluate D_N it is appropriate to introduce the Hermitian Wilson-Dirac operator $H_W(\rho) = \gamma_5 D_W(\rho)$, such that

$$D_N = \frac{\rho}{a}(1 + \gamma_5 \mathrm{sgn}\{H_W(\rho)\}), \tag{3}$$

where $\mathrm{sgn}\{H\} = H/\sqrt{H^2}$. The sign function can be defined by means of the spectral decomposition

$$\mathrm{sgn}\{H_W(\rho)\} = \sum_i \mathrm{sgn}\{\mu_i\}\chi_i\chi_i^\dagger, \tag{4}$$

where χ_i are the normalized eigenvectors of $H_W(\rho)$ with eigenvalue μ_i. Equation (4) is not, however, suitable for numerical evaluation. We write

$$\mathrm{sgn}\{H_W(\rho)\} = \sum_{i=1}^{N} \mathrm{sgn}\{\mu_i\}\chi_i\chi_i^\dagger + P_\perp^N \mathrm{sgn}\{H_W(\rho)\}, \tag{5}$$

where

$$P_\perp^N = 1 - \sum_{i=1}^{N} \chi_i\chi_i^\dagger \tag{6}$$

projects onto the subspace orthogonal to the eigenvectors of the N lowest eigenvalues of $|H_W(\rho)|$, and approximate $P_\perp^N \mathrm{sgn}\{H_W(\rho)\}$ by a minmax polynomial [14]. More precisely, we construct a polynomial $P(x)$, such that

$$\left| P(x) - \frac{1}{\sqrt{x}} \right| < \epsilon, \qquad x \in [\mu_{N+1}^2, \mu_{\max}^2], \tag{7}$$

where μ_{N+1} ($\mu_{\max}$) is the lowest nonzero (largest) eigenvalue of $|P_\perp^N H_W(\rho)|$. We then have

$$\mathrm{sgn}\{H_W(\rho)\} = \sum_{i=1}^{N} \mathrm{sgn}\{\mu_i\}\chi_i\chi_i^\dagger + P_\perp^N H_W(\rho) P(H_W^2(\rho)). \tag{8}$$

The degree of the polynomial will depend on ϵ and on the condition number of $H_W^2(\rho)$, $\kappa = \mu_{\max}^2/\mu_{N+1}^2$, on the subspace $\{\chi_i | (1 - P_\perp^N)\chi_i = 0\}$.

We use the Lüscher-Weisz gauge action [15]

$$\begin{aligned} S[U] = \frac{6}{g^2}\Bigg[& c_0 \sum_{\text{plaquette}} \frac{1}{3}\,\mathrm{Re\,Tr}(1 - U_{\text{plaquette}}) \\ & + c_1 \sum_{\text{rectangle}} \frac{1}{3}\,\mathrm{Re\,Tr}(1 - U_{\text{rectangle}}) \\ & + c_2 \sum_{\text{parallelogram}} \frac{1}{3}\,\mathrm{Re\,Tr}(1 - U_{\text{parallelogram}}) \Bigg], \end{aligned} \tag{9}$$

where $U_{\text{plaquette}}$ is the standard plaquette, $U_{\text{rectangle}}$ denotes the closed loop along the links of the 1×2 rectangle, and $U_{\text{parallelogram}}$ denotes the closed loop along the diagonally opposite links of the cubes. The coefficients c_1, c_2 are taken from tadpole improved perturbation theory [16]:

$$\frac{c_1}{c_0} = -\frac{(1 + 0.4805\alpha)}{20u_0^2}, \qquad \frac{c_2}{c_0} = -\frac{0.033\,25\alpha}{u_0^2} \tag{10}$$

with $c_0 + 8c_1 + 8c_2 = 1$, where

$$u_0 = \left(\frac{1}{3}\,\mathrm{Tr}\langle U_{\text{plaquette}}\rangle\right)^{1/4}, \qquad \alpha = -\frac{\log(u_0^4)}{3.068\,39}. \tag{11}$$

We write

$$\beta = \frac{6}{g^2}c_0. \tag{12}$$

After having fixed β, the parameters c_1, c_2 are determined. In the classical continuum limit $u_0 \to 1$ the coefficients c_1, c_2 assume the tree-level Symanzik values [17] $c_1 = -1/12$, $c_2 = 0$. The Lüscher-Weisz action suppresses unphysical zero modes, called dislocations [18], and is perturbatively much better motivated than the Iwasaki and DBW2 gauge actions [19] (in combination with overlap fermions).

III. SIMULATION PARAMETERS

The simulations are done on lattices listed in Table I. The scale parameter r_0/a was taken from [16]. The couplings have been chosen such that the $16^3 32$ lattice at $\beta = 8.0$ and the $24^3 48$ lattice at $\beta = 8.45$ have approximately the same physical volume. This allows us to study both scaling violations and finite size effects.

We have projected out $N = 40$ lowest lying eigenvectors at $\beta = 8.0$ and $N = 50$ ($N = 10$) at $\beta = 8.45$ on the $24^3 48$ ($16^3 32$) lattice. These numbers scale roughly with the physical volume of the lattice. We used the Arnoldi method to compute eigenvalues and eigenvectors. The degree of the polynomial P has been adjusted such that $1/\sqrt{H_W^2(\rho)}$ is determined with a relative accuracy of better than 10^{-7}.

The mass parameter ρ influences the simulation in two ways. First, it affects the locality properties [8] of the Neuberger-Dirac operator. In Fig. 1 we show the effective range of D_N,

$$F(r) = \langle\langle \max_x |D_N(x, y)| \rangle_{||x-y||=r}\rangle_y\rangle_U, \tag{13}$$

TABLE I. Lattices.

β	Volume	r_0/a
8.00	$16^3 32$	3.69(4)
8.45	$16^3 32$	5.29(7)
8.45	$24^3 48$	5.29(7)

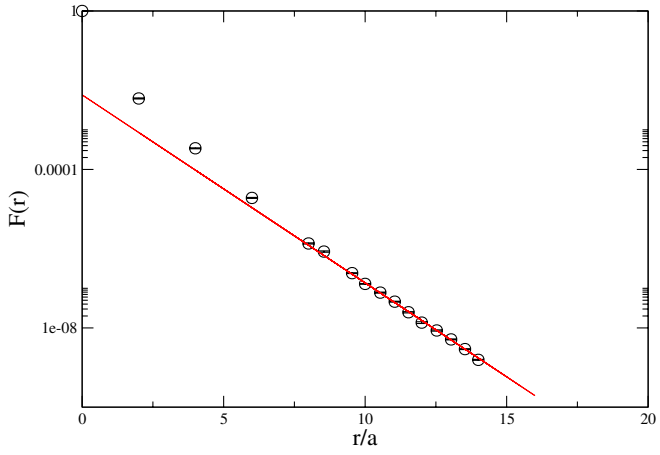

FIG. 1 (color online). The effective range $F(r)$ as a function of r/a on the $16^3 32$ lattice at $\beta = 8.45$ for $\rho = 1.4$, together with an exponential fit. The fit gave $\mu = 1.11(1)$.

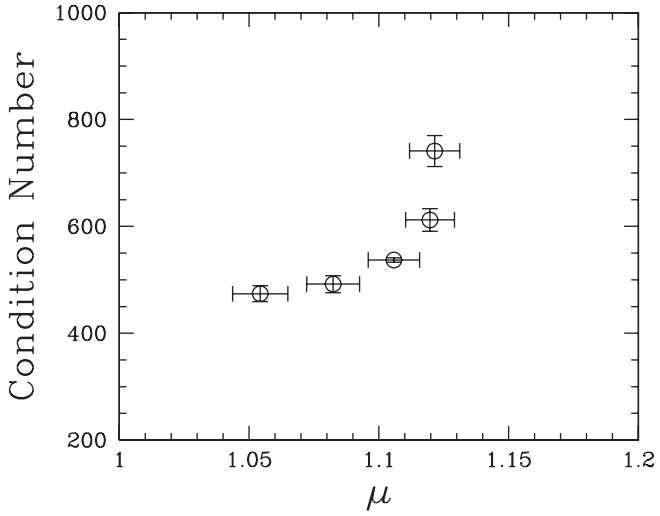

FIG. 2. Condition number and μ on the $16^3 32$ lattice at $\beta = 8.45$ for $\rho = 1.2$, 1.3, 1.4, 1.5, and 1.6, from left to right.

with respect to the Euclidean distance

$$\|x\| = \left(\sum_{\mu=1}^{4} x_\mu^2\right)^{1/2}. \tag{14}$$

Asymptotically, $F(r) \propto \exp(-\mu r/a)$, where μ depends (among others) on ρ. (Numerically, $\mu \approx 2\nu$, where ν refers to the taxi-driver distance [8].) We want μ to be as large as possible, in particular, $2\mu \gg m_H a$ ($3\mu \gg m_H a$) for mesons (baryons). Second, the condition number of $P_\perp^N H_W^2(\rho)$, $\kappa = \mu_{\max}^2/\mu_{N+1}^2$, depends on ρ as well. In Fig. 2 we show the ρ dependence of μ and κ on the $16^3 32$ lattice at $\beta = 8.45$ for $N = 10$. Test runs show, however, that κ does not decrease significantly anymore if we increase N further. We have chosen $\rho = 1.4$, which is a trade-off between a small condition number κ and a large value of μ. At this value of ρ we find $\mu = 1.11(1)$, which is consistent with the results obtained in [8] from the Wilson gauge action.

The simulations are performed at the quark masses listed in Table II. This covers the range of pseudoscalar masses $250 \lesssim m_{\rm PS} \lesssim 900$ MeV as we shall see. The lowest quark mass was chosen such that $m_{\rm PS} L \gtrsim 3$ (L being the spatial extent of the lattice). On all our lattices we have $L \gg 1/(2f_\pi)$.

$O(a)$ improvement, both for masses and on- and off-shell operator matrix elements, is achieved by simply replacing D in (1) by [3]

$$D^{\rm imp} \equiv \left(1 - \frac{am_q}{2\rho}\right) D \left(1 - \frac{a}{2\rho} D\right)^{-1} \tag{15}$$

in the calculation of the quark propagator. Apart from the multiplicative mass term, this amounts to subtracting the contact term from the propagator. In the following we shall always use the improved propagator, without mentioning it explicitly. The eigenvalues of D_N lie on a circle of radius ρ/a around $(\rho/a, 0)$ in the complex plane, while the eigenvalues of the improved operator $D_N^{\rm imp} = D_N(1 - \frac{a}{2\rho} D_N)^{-1}$ lie on the imaginary axis.

IV. HADRON MASSES AND PSEUDOSCALAR DECAY CONSTANT

Let us now turn to the calculation of hadron masses and the pseudoscalar decay constant. Before we can compare our results with the real world, we have to set the scale. We will use the pion decay constant to do so, for reasons which will become clear later. The pion decay constant derives from the axial vector current, which has to be renormalized in the process.

A. Calculational details

The coefficients c_1, c_2 of the gauge field action are [16] $c_1 = -0.169\,805$, $c_2 = -0.016\,341\,4$ at $\beta = 8.0$ and $c_1 = -0.154\,846$, $c_2 = -0.013\,407\,0$ at $\beta = 8.45$. For

TABLE II. Mass parameters.

β	V	am_q						
8.00	$16^3 32$	0.0168	0.0280	0.0420	0.0560	0.0840	0.1400	0.1960
8.45	$16^3 32$				0.0280	0.0560	0.0980	0.1400
8.45	$24^3 48$		0.0112	0.0196	0.0280	0.0560	0.0980	0.1400

the gauge field update we use a heat bath algorithm, which we repeat 1000 times to generate a new configuration.

The inversion of the overlap operator D is done by solving the system of equations

$$Ax = y, \tag{16}$$

where $A = D^\dagger D$ and y is the relevant source vector. We use the conjugate gradient algorithm for that. The speed of convergence depends on the condition number of the operator A, $\kappa(A) = \nu_{\max}/\nu_{\min}$, where $\nu_{\max}$ ($\nu_{\min}$) is the largest (lowest) eigenvalue of A. For reasonable values of the quark mass we have $\kappa(A) \propto 1/m_q^2$. Thus, the number of iterations, n_D, needed to achieve a certain accuracy will grow like $n_D \propto 1/m_q$ as the quark mass is decreased.

The convergence of the algorithm can be accelerated by a preconditioning method. Instead of (16) we solve the equivalent system of equations

$$ACx = Cy \equiv \tilde{A}x, \tag{17}$$

where C is a nonsingular matrix, which we choose such that $\kappa(\tilde{A}) \ll \kappa(A)$. Our choice is

$$C = 1 + \sum_{i=1}^{n}\left(\frac{1}{\nu_i} - 1\right)v_i v_i^\dagger, \tag{18}$$

where v_i (ν_i) are the normalized eigenvectors (eigenvalues) of A. The condition number of the operator $\tilde{A}$ is by a factor ν_{n+1}/ν_1 smaller than the condition number of the operator A, and the number of iterations in the conjugate gradient algorithm reduces to $n_D \propto 1/\sqrt{\nu_{n+1} + m_q^2}$, which depends only weakly on the quark mass m_q. We have chosen $n = 80$, and the inversion was stopped when a relative accuracy of 10^{-7} was reached. We have checked that increasing the accuracy does not change the correlation functions for all our quark masses.

In the calculation of meson and baryon correlation functions we use smeared sources to improve the overlap with the ground state, while the sinks are taken to be either smeared or local. We use Jacobi smearing for source and sink [20]. To set the size of the source, we have chosen $\kappa_s = 0.21$ for the smearing hopping parameter and employed $N_s = 50$ smearing steps.

To further improve the signal of the correlation functions, we have deployed low-mode averaging [21] in some cases by breaking the quark propagator into two pieces,

$$\sum_{i=1}^{n_\ell} \frac{\psi_i(x)\psi_i^\dagger(y)}{\lambda_i^{\text{imp}} + m_q}, \tag{19}$$

where the sum extends over the eigenmodes of the n_ℓ lowest eigenvalues of D_N^{imp}, and the remainder. The contribution from the low-lying modes (19) is averaged over all positions of the quark sources. As the largest contribution to the correlation functions comes from the lower modes, we may expect a significant improvement in the regime of small quark masses. We have chosen $n_\ell = 40$, mainly because of memory limitations.

B. Lattice results

The calculations are based on 900–1300 gauge field configurations at the lowest four quark masses at $\beta = 8.0$, and on 200–300 configurations elsewhere. We consider hadrons only with all quarks having degenerate masses.

1. Pion mass

To compute the pseudoscalar mass, m_{PS}, we looked at correlation functions of the pseudoscalar density $P = \bar{\psi}\gamma_5\psi$ and the time component of the axial vector current $A_4 = \bar{\psi}\gamma_4\gamma_5\psi$. In Fig. 3 we show the corresponding effective mass for our four lowest quark masses on the $24^3 48$ lattice. Local sinks are found to give slightly smaller error bars than smeared sinks, so that we will restrict ourselves to this case. Both correlators give consistent results. We will use the results from the axial vector current correlator here, because it results in a wider plateau as the pseudoscalar correlator, in particular, at the larger quark masses. We fit the correlator by the function $A\cosh(m_{\text{PS}}(t - T/2))$, where T is the temporal extent of the lattice, over the region of the plateau. The results of the fit are listed in Table III.

2. Rho and nucleon masses

To compute the vector meson mass, m_V, we explored correlation functions of operators $V_i = \bar{\psi}\gamma_i\psi$ and $V_i^4 = \bar{\psi}\gamma_i\gamma_4\psi$ ($i = 1, 2, 3$). We found that the operator V_i, in combination with a local sink, gives the best signal. In Fig. 4 we show the effective rho mass for all six quark masses on the $24^3 48$ lattice.

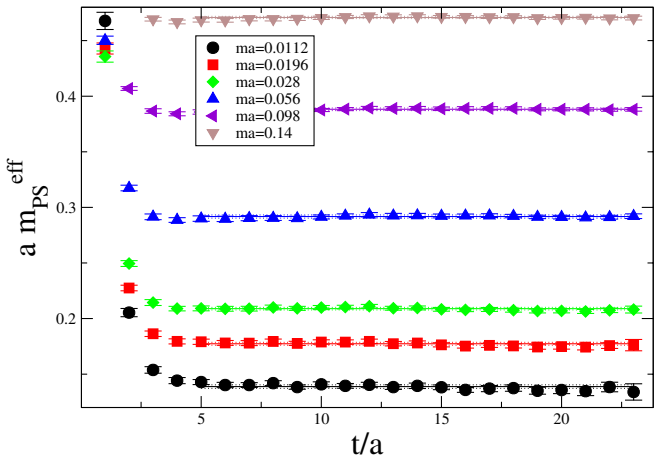

FIG. 3 (color online). The effective pseudoscalar mass from the correlation function of the axial vector current A_4 on the $24^3 48$ lattice at $\beta = 8.45$, using smeared sources and local sinks.

TABLE III. Hadron masses and pseudoscalar decay constant. The numbers marked by $*$ are obtained with low-mode averaging. To convert $m_{\rm PS}$ to physical units, we have used the result in Table IV. The error on $m_{\rm PS}$ in the last column is purely statistical.

β	V	am_q	$am_{\rm PS}$	am_V	am_N	$af_{\rm PS}$	$m_{\rm PS}$ (MeV)
8.00	$16^3 32$	0.0168	0.190(1)	0.643(5)	0.793(5)	0.075(1)	239(1)
		0.0280	0.235(1)	0.64935)	0.821(4)	0.076(1)	295(1)
		0.0420	0.281(1)	0.65923)	0.863(3)	0.078(1)	353(1)
		0.0560	0.321(1)	0.669(2)	0.890(3)	0.080(1)	403(1)
		0.0840	0.388(1)	0.695(3)	0.952(7)	0.082(1)	488(1)
		0.1400	0.502(1)	0.751(2)	1.074(7)	0.090(1)	631(1)
		0.1960	0.599(1)	0.815(1)	1.188(7)	0.097(1)	753(1)
8.45	$16^3 32$	0.0280	0.212(3)	0.441(6)*	0.595(6)*	0.053(1)	396(8)
		0.0560	0.289(2)	0.482(4)*	0.675(4)*	0.058(1)	545(4)
		0.0980	0.384(2)	0.537(4)	0.784(7)	0.064(1)	727(4)
		0.1400	0.467(2)	0.595(3)	0.886(6)	0.070(1)	883(4)
8.45	$24^3 48$	0.0112	0.139(1)	0.429(6)*	0.551(12)*	0.051(1)	264(4)
		0.0196	0.177(1)	0.442(6)*	0.572(11)*	0.052(1)	336(2)
		0.0280	0.209(1)	0.452(3)*	0.600(10)*	0.054(1)	396(2)
		0.0560	0.292(1)	0.481(3)	0.674(12)	0.058(1)	551(2)
		0.0980	0.388(1)	0.538(2)	0.788(11)	0.065(1)	731(2)
		0.1400	0.412(1)	0.597(1)	0.892(11)	0.071(1)	887(2)

For the calculation of the nucleon mass, m_N, we used $B_\mu = \varepsilon_{abc}\psi^a_\mu(\psi^b C\gamma_5\psi^c)$ (where $C = \gamma_4\gamma_2$) as our basic operator, where we have replaced each spinor by $\psi \to \psi^{\rm NR} = (1/2)(1+\gamma_4)\psi$ [20]. These so-called nonrelativistic wave functions have a better overlap with the ground state than the ordinary, relativistic ones. In Fig. 5 we show the effective nucleon mass for our six quark masses on the $24^3 48$ lattice, where for the lowest three quark masses we have employed low-mode averaging. We find good to reasonable plateaus starting at $t/a \gtrsim 8$. In Fig. 6 we show, for comparison, the result obtained without low-mode averaging. In this case the situation is less favorable. The nucleon mass is obtained from a fit of the data by the correlation function $A\exp(-m_N t) + B\exp(-m_{N^*}(T-t))$, where m_{N^*} is the mass of the backward moving baryon, over the region of the plateau. The relative error on the nucleon propagator is expected to grow [22] $\propto \exp[(m_N - 3m_{\rm PS}/2)t]/\sqrt{N}$, N being the number of configurations, as t increases and/or $m_{\rm PS}$ decreases, and that is what we observe.

The results for the rho and nucleon masses are listed in Table III. Note that $am_V \ll 2\mu$ and $am_N \ll 3\mu$, respectively, are satisfied in all cases. In Fig. 7 we show an APE

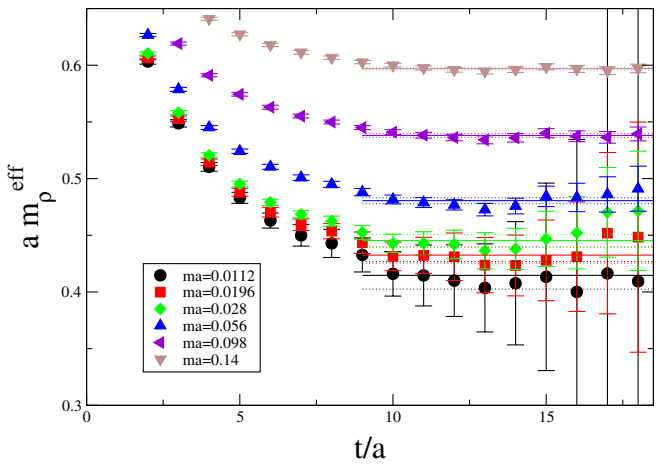

FIG. 4 (color online). The effective rho mass on the $24^3 48$ lattice at $\beta = 8.45$, using smeared sources and local sinks. The horizontal lines indicate the fit interval as well as the value and error of the mass.

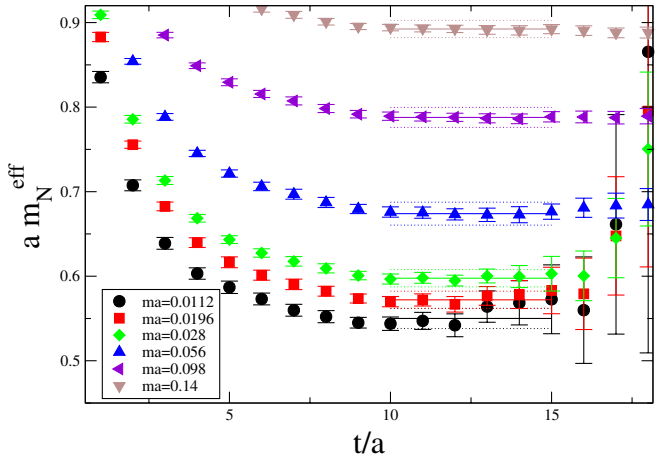

FIG. 5 (color online). The effective nucleon mass on the $24^3 48$ lattice at $\beta = 8.45$, using smeared sources and local sinks. The horizontal lines indicate the fit interval as well as the value and error of the mass. The data points at the lowest three quark masses have been computed with low-mode averaging.

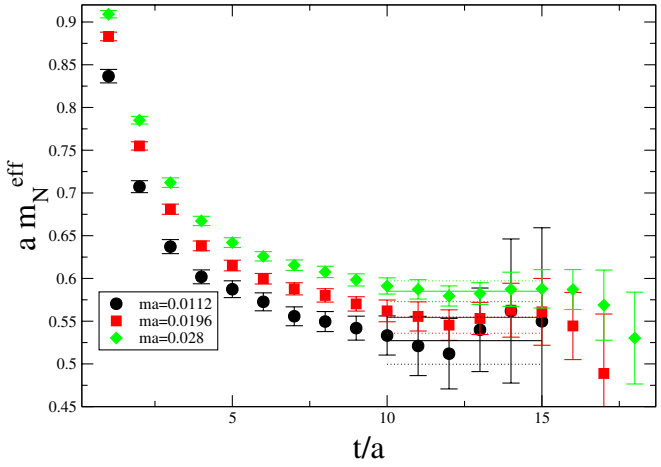

FIG. 6 (color online). The same as the previous figure, but for the lowest three quark masses without using low-mode averaging.

plot for our three lattices. At our smallest quark masses we have $m_{\rm PS}/m_V \approx 0.3$. The APE plot shows no scaling violations outside the error bars and no finite size effects.

3. Pion decay constant

The physical pion decay constant is given by

$$\langle 0|\mathcal{A}_4|\pi\rangle = m_\pi f_\pi, \tag{20}$$

where $\mathcal{A}_\mu$ is the renormalized axial vector current, $\mathcal{A}_\mu = Z_A A_\mu$. Using the axial Ward identity

$$\partial_\mu \mathcal{A}_\mu = 2m_q P, \tag{21}$$

where P is the *local* pseudoscalar density, and considering the fact that $m_q P$ is a renormalization group invariant, we obtain

$$f_\pi = \frac{2m_q}{m_\pi^2}\langle 0|P|\pi\rangle. \tag{22}$$

On the lattice we consider the correlation function

$$\begin{aligned}\langle P^s(t)P^{s'}(0)\rangle &= \frac{1}{2am_{\rm PS}}\langle 0|P^s|PS\rangle\langle PS|P^{s'}|0\rangle \\ &\quad\times[\exp(-m_{\rm PS}t)+\exp(-m_{\rm PS}(T-t))] \\ &\equiv A^{ss'}[\exp(-m_{\rm PS}t)+\exp(-m_{\rm PS}(T-t))],\end{aligned} \tag{23}$$

where the superscripts s, s' distinguish between local (L) and smeared (S) operators. From this we obtain [23]

$$af_{\rm PS} = \frac{2am_q}{(am_\pi)^{3/2}}\frac{A^{LS}}{\sqrt{A^{SS}}}. \tag{24}$$

We thus find $af_{\rm PS}$ by computing A^{LS} and A^{SS}. In Table III we give our results. In our notation the experimental value of f_π is 92.4 MeV.

Comparing our data on the $16^3 32$ and $24^3 48$ lattices at $\beta = 8.45$ in Table III piece by piece, we also find no finite size effects down to the lowest common pseudoscalar mass.

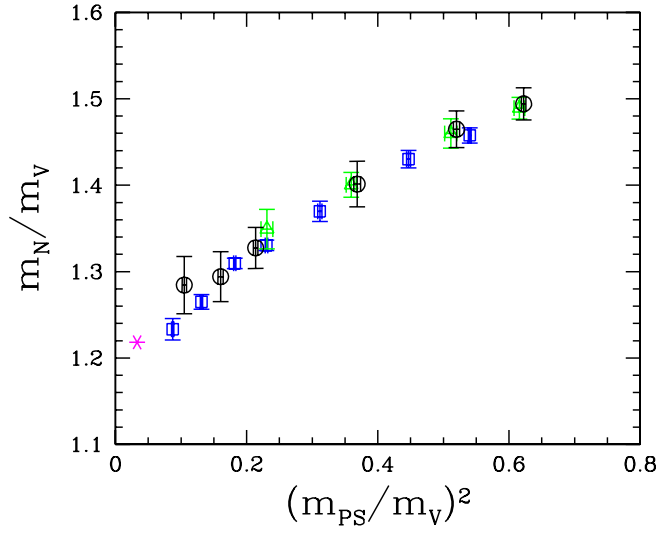

FIG. 7 (color online). APE plot on the $24^3 48$ lattice at $\beta = 8.45$ (○) and on the $16^3 32$ lattices at $\beta = 8.0$ (□) and $\beta = 8.45$ (△), together with the experimental value (∗).

C. Setting the scale: Pion decay constant

We will use the pseudoscalar decay constant to set the scale. The reason is that $f_{\rm PS}$ is an analytic function in $m_{\rm PS}^2$ for degenerate quark masses [24], in contrast to m_V and m_N, which exhibit nonanalytic behavior. We thus expect that $f_{\rm PS}$ extrapolates smoothly to the chiral limit. In quenched chiral perturbation theory [25,26] to NLO we have[1] [24]

$$f_{\rm PS} = f_0\left(1+\alpha_5^q\frac{m_{\rm PS}^2}{2(4\pi f_0)^2}\right)+O(m_{\rm PS}^4). \tag{25}$$

In Fig. 8 we show our data together with a quartic fit in the pseudoscalar mass. The lattice spacing is obtained from requiring $f_{\rm PS} = f_\pi = 92.4$ MeV at the physical pion mass. Using the r_0/a values given in Table I, we can convert the lattice spacing a into the dimensionful scale parameter r_0. The results of the fits are compiled in Table IV. Note that α_5^q, f_0, and r_0 come out independent of the lattice spacing within the error bars, which, once more, indicates good scaling properties of our action. The coefficient α_5^q turns out to be in agreement with the phenomenological value of 1.83 ($L_5^q = 0.001\,45$) reported in [28].

[1]Here and in the following we shall adopt the notation $\alpha_i = 128\pi^2 L_i$, α_i (L_i) being the familiar (conventional) Gasser-Leutwyler coefficients [27]. The superscript q stands for quenched.

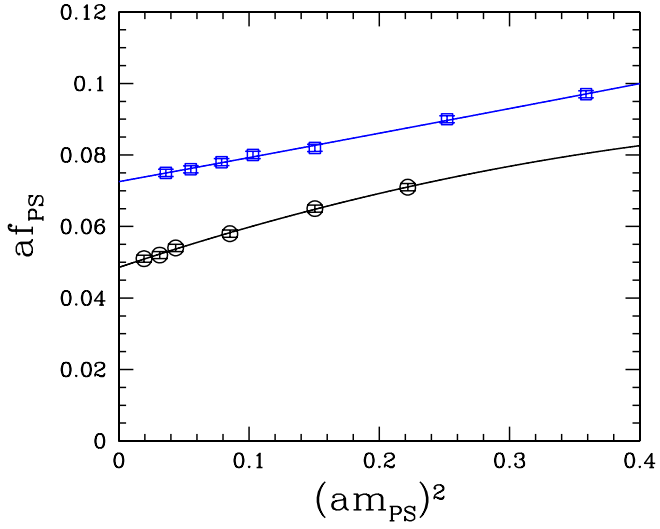

FIG. 8 (color online). Chiral extrapolation of the pseudoscalar decay constant on the $24^3 48$ lattice at $\beta = 8.45$ (○) and on the $16^3 32$ lattice at $\beta = 8.0$ (□).

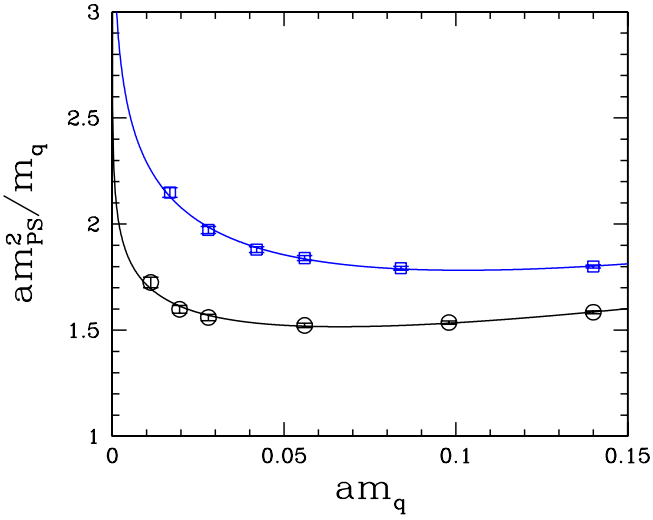

FIG. 9 (color online). Chiral extrapolation of the pseudoscalar mass on the $24^3 48$ lattice at $\beta = 8.45$ (○) and on the $16^3 32$ lattice at $\beta = 8.0$ (□). The curves show the fits for $\alpha^q_\Phi = 0$.

TABLE IV. The pion decay constant.

β	V	af_0	α^q_5	a (fm)	f_0 (MeV)	r_0 (fm)
8.00	$16^3 32$	0.073(1)	1.5(4)	0.157(3)	92(1)	0.58(2)
8.45	$24^3 48$	0.049(1)	1.9(4)	0.105(2)	91(2)	0.56(2)

D. Comparison with chiral perturbation theory

We shall now compare our results for the pseudoscalar, vector meson, and nucleon masses with the predictions of chiral perturbation theory and attempt to extrapolate the lattice numbers to the chiral limit.

1. Pion mass

We plot the pseudoscalar masses as a function of the quark mass in Fig. 9. Quenched chiral perturbation theory [25] predicts in the infinite volume [24,29]

$$\frac{m^2_{\rm PS}}{m_q} = A\Big\{1 - \Big(\delta - \frac{2}{3}\alpha^q_\Phi y\Big)(\ln y + 1) + \Big[(2\alpha^q_8 - \alpha^q_5) - \frac{\alpha^q_\Phi}{3}\Big]y\Big\} + \cdots \quad (26)$$

with

$$y = \frac{Am_q}{\Lambda^2_\chi} \quad (27)$$

where $A = 2\Sigma/f_0^2$, Σ being the "bare quark condensate," and Λ_χ denotes the scale at which the α_i's are being evaluated. The traditional value is $\Lambda_\chi = 4\pi f_0$, which we will also adopt here. For the parameter δ chiral perturbation theory predicts [25,26]

$$\delta = \frac{\mu_0^2}{48\pi^2 f_\pi^2}, \quad (28)$$

with $\mu_0^2 \equiv m^2_{\eta'} + m^2_\eta - 2m^2_K = (870\ \text{MeV})^2$. This gives $\delta = 0.183$. The parameters f_0 and α^q_5 are known from our fit of $f_{\rm PS}$ and are given in Table IV.

A much sought after quantity is the parameter δ. Though unphysical, it would be a great success of the calculation, and of quenched chiral perturbation theory as well, if δ turned out to be in agreement with the predicted value. We shall try to determine δ directly from the data. Let us write

$$z = \frac{m^2_{\rm PS}}{\Lambda^2_\chi}, \qquad w = \frac{m^2_{\rm PS}}{m_q} \quad (29)$$

and introduce the effective δ parameter

$$\delta^{-1}_{\rm eff} = 1 + \frac{\ln z' w - \ln z w'}{w - w'}, \quad (30)$$

where z, z' and w, w', respectively, are adjacent data points. It is easy to see that

$$\lim_{m_q \to 0} \delta_{\rm eff} = \delta. \quad (31)$$

In Fig. 10 we show $\delta_{\rm eff}$ as a function of the quark mass. In the case of our high statistics run on the $16^3 32$ lattice at $\beta = 8.0$, we are able to extrapolate $\delta_{\rm eff}$ to the chiral limit. We obtain $\delta = 0.18(4)$, in agreement with the prediction of quenched chiral perturbation theory. On the $24^3 48$ lattice at $\beta = 8.45$, our current statistics does not allow such an extrapolation. But the data for $\delta_{\rm eff}$ are consistent with the predicted value of δ.

The Witten-Veneziano formula [30] relates μ_0^2 to the topological susceptibility

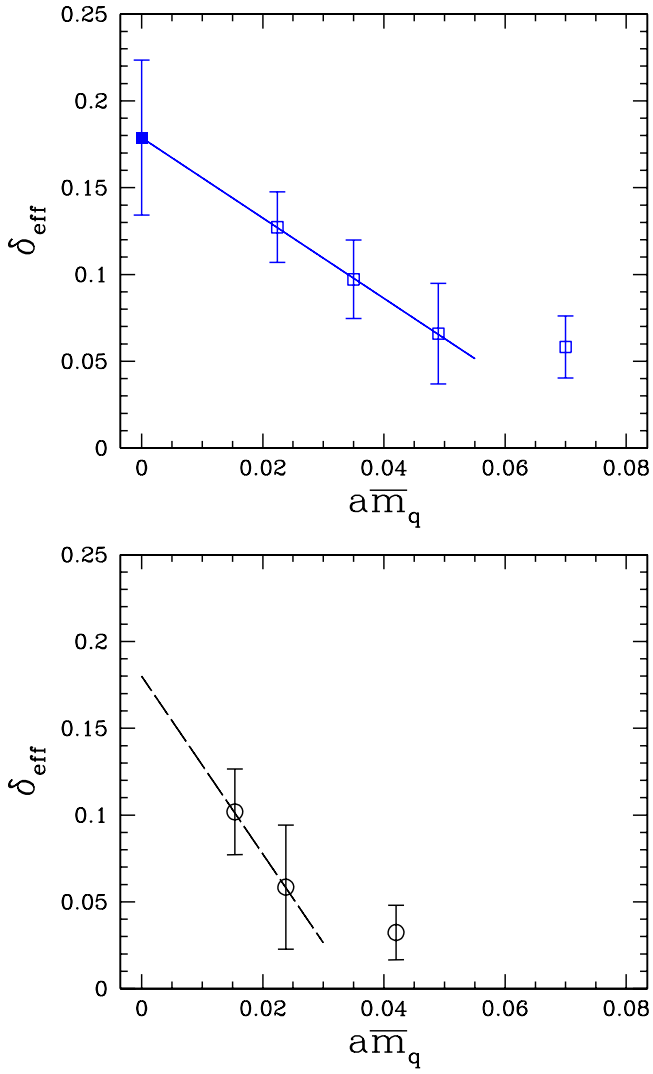

FIG. 10 (color online). The parameter $\delta_{\rm eff}$ on the $16^3 32$ lattice at $\beta = 8.0$ together with a linear fit (top panel) and on the $24^3 48$ lattice at $\beta = 8.45$ (bottom panel), as a function of the average quark mass $\bar{m}_q = (m_q + m'_q)/2$.

$$\chi_t = \frac{\langle Q^2 \rangle}{V}, \tag{32}$$

where Q is the topological charge and V the lattice volume. The result for δ is

$$\delta = \frac{1}{8\pi^2 f_\pi^4} \chi_t, \tag{33}$$

which suggests that the pseudoscalar mass depends on the topological charge $|Q|$. This turns out to be indeed the case. In Fig. 11 we show the pseudoscalar mass for various charge sectors, where the charge Q is given by the index ν of D_N. We observe a strong increase of δ with increasing $|Q|$, and contrary to the findings in [31], we do not expect the effect to go away in the limit $V \to \infty$, χ_t fixed. It would be interesting to search other quantities for a $|Q|$ dependence as well.

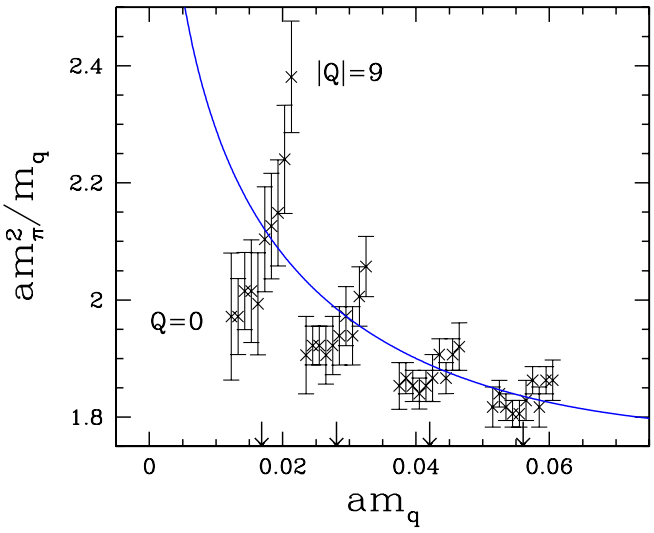

FIG. 11 (color online). The pseudoscalar mass on the $16^3 32$ lattice at $\beta = 8.0$ for $|Q| = 0, \ldots, 9$, from left to right. The data have been displaced horizontally. The true quark masses are indicated by the arrow at the bottom rim of the figure. The curve is from Fig. 9.

Let us now turn to the fit of (26) to the data. Knowing f_0 and α_5^q, this leaves us with four free parameters. Because our data do not allow an uncorrelated fit of all four parameters, we have to make a choice and fix one of them. We consider two cases. In the first case we fix α_Φ at 0, while in the second case we fix δ at its theoretical value of 0.183. The results of both fits are compiled in Table V, where we have omitted the heaviest mass point at $\beta = 8.00$. The numbers shown in *italics* are the numbers that we fixed. It is not expected that A scales. Assuming $\delta = 0.183$ and taking f_0 from Table IV, we obtain $a^3\Sigma = 0.0039(1)$ at $\beta = 8.0$ and $a^3\Sigma = 0.001\,38(5)$ at $\beta = 8.45$, respectively. We shall return to Σ and the fit function (26) when we compute the renormalized chiral condensate and quark masses. Combining the results on both lattices, we obtain $a_8^q = 1.5(4)$ for $\delta = 0.183$. This is to be compared with [29] $a_8 = 0.8(4)$ in full QCD. In Fig. 9 we compare the fits with the data.

Alternatively, one may fit the low-lying pseudoscalar masses by the resummed expression [26] $m_{\rm PS}^2/m_q = Ay^{-\delta/(1+\delta)}$. A fit to the lowest three data points gives $\delta = 0.17(2)$ on the $16^3 32$ lattice at $\beta = 8.0$ and $\delta = 0.12(2)$ on the $24^3 48$ lattice at $\beta = 8.45$, respectively.

TABLE V. The pion mass.

β	V	aA	δ	α_Φ^q	α_8^q	χ^2/dof
8.00	$16^3 32$	1.0(1)	0.34(7)	0.0	1.4(6)	0.8
		1.46(2)	0.183	0.8(2)	1.5(2)	1.3
8.45	$24^3 48$	1.22(4)	0.16(2)	0.0	1.3(2)	1.0
		1.15(2)	0.183	−0.2(1)	1.4(4)	0.8

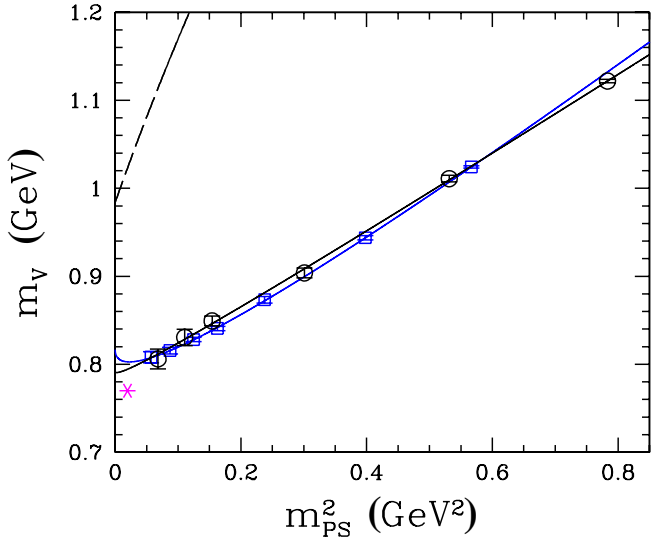

FIG. 12 (color online). Chiral extrapolation of the vector meson mass on the $24^3 48$ lattice at $\beta = 8.45$ (○) and on the $16^3 32$ lattice at $\beta = 8.0$ (□), together with the experimental value ($*$). The solid curves show the fits. The dashed curve in the top left corner shows the energy of the state of two pseudoscalar mesons.

2. Rho mass

In Fig. 12 we plot the vector meson masses as a function of the pseudoscalar mass, where we have used the results of Table IV to convert the lattice numbers to physical values. Quenched chiral perturbation theory predicts [32]

$$m_V = C_0^V + C_{1/2}^V m_{\rm PS} + C_1^V m_{\rm PS}^2 + C_{3/2}^V m_{\rm PS}^3 + \cdots, \quad (34)$$

where $m_{\rm PS}$ is the lattice pseudoscalar mass as described by (26). The coefficient $C_{1/2}^V$ is expected to be negative, so that the chiral limit is approached from below. Our data show no indication of a cubic term, and so we shall drop that. The results of a quadratic fit in the pseudoscalar are given in Table VI. Our high statistics run at $\beta = 8.0$ indeed gives a negative value for $C_{1/2}$, but perhaps of lower magnitude than expected [32], while at $\beta = 8.45$ our statistics is not high enough to make any statement. The fits are shown in Fig. 12. One might think that at the lighter quark masses one is seeing the lowest two-pion state instead of the rho. In Fig. 12 we also show the energy of two pseudoscalar mesons at the lowest nonvanishing lattice momentum,[2] $|p| = 2\pi/(aL)$, assuming the lattice dispersion relation to hold. We see that the lowest two-pion energy lies well above the vector meson mass because of the finite size of our lattice.

3. Nucleon mass

We plot the nucleon masses as a function of the pseudoscalar mass in Fig. 13. Quenched chiral perturbation theory predicts [33]

$$m_N = C_0^N + C_{1/2}^N m_{\rm PS} + C_1^N m_{\rm PS}^2 + C_{3/2}^N m_{\rm PS}^3 + \cdots, \quad (35)$$

where

$$C_{1/2}^N = -\tfrac{3}{2}(3F - D)^2 \pi \delta. \quad (36)$$

Assuming the tree-level values $F = 0.50$ and $D = 0.76$, we expect $C_{1/2}^N = -2.58\delta$. For the theoretical value $\delta = 0.183$ this would give $C_{1/2}^N = -0.47$. Of course, F and D may be different in the quenched theory. In the $N_c \to \infty$ limit, for example, $F/D = 1/3$ giving $C_{1/2}^N = 0$. Again, our data show no indication of a cubic term, and we shall drop that here as well. The results of a quadratic fit in the pseudoscalar mass are given in Table VII. At $\beta = 8.0$ we find some evidence for nonanalytic behavior, but with a positive coefficient $C_{1/2}^N$. The fits are shown in Fig. 13.

TABLE VI. The rho mass.

β	V	C_0^V (GeV)	$C_{1/2}^V$	C_1^V (GeV^{-1})
8.00	$16^3 32$	0.82(1)	−0.18(5)	0.61(5)
8.45	$24^3 48$	0.79(2)	−0.05(7)	0.48(6)

TABLE VII. The nucleon mass.

β	V	C_0^N (GeV)	$C_{1/2}^N$	C_1^N (GeV^{-1})
8.00	$16^3 32$	0.87(2)	0.4(1)	0.6(1)
8.45	$24^3 48$	0.90(7)	0.3(3)	0.6(2)

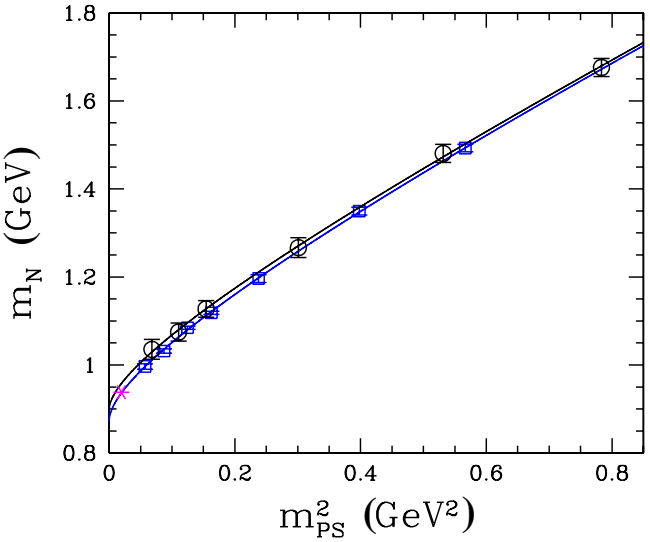

FIG. 13 (color online). Chiral extrapolation of the nucleon mass on the $24^3 48$ lattice at $\beta = 8.45$ (○) and on the $16^3 32$ lattice at $\beta = 8.0$ (□), together with the experimental value ($*$). The curves show the fits.

[2]Note that the pions in the rho are in a relative p wave.

Figure 13 corroborates once more that it is important to have data at small quark masses to reliably extrapolate to the chiral limit. For example, a linear extrapolation of data limited to $m_{\rm PS} \gtrsim 500$ MeV, as exercised in many previous quenched calculations, would result in a 10%–20% larger nucleon mass at the physical pion mass.

To sum up, we find a typical behavior for quenched QCD, with some results (e.g. m_N) apparently being in reasonable agreement with the experimental value, while others (e.g. m_V) show a disagreement. Both m_V and m_N scale, within the error bars, with the inverse lattice spacing set by the pion decay constant f_π.

V. NONPERTURBATIVE RENORMALIZATION

We shall now turn to the determination of the renormalization constants Z_S, Z_P, and Z_A of the scalar and pseudoscalar densities and the axial vector current, respectively, which we will need in order to compute the renormalized quark mass. We shall employ the RI′-MOM scheme [34]. Our implementation of this method is described in [35].

We consider amputated Green functions, or vertex functions, $\Gamma_{\mathcal{O}}$, with operator insertion $\mathcal{O} = S$, P and A_4 in the Landau gauge. Defining renormalized vertex functions by

$$\Gamma^R_{\mathcal{O}}(p) = Z_q(\mu)^{-1} Z_{\mathcal{O}}(\mu) \Gamma_{\mathcal{O}}(p), \tag{37}$$

where μ is the renormalization scale, we fix the renormalization constants by imposing the renormalization condition

$$\frac{1}{12} \mathrm{Tr}[\Gamma^R_{\mathcal{O}}(p) \Gamma^{-1}_{\mathcal{O},\mathrm{Born}}]|_{p^2=\mu^2} = 1. \tag{38}$$

That is, we compute the renormalization constants from

$$Z_q(\mu)^{-1} Z_{\mathcal{O}}(\mu) \frac{1}{12} \mathrm{Tr}[\Gamma_{\mathcal{O}}(p) \Gamma^{-1}_{\mathcal{O},\mathrm{Born}}]|_{p^2=\mu^2} \equiv Z_q(\mu)^{-1} Z_{\mathcal{O}}(\mu) \Lambda_{\mathcal{O}}(p)|_{p^2=\mu^2} = 1 \tag{39}$$

with $\Gamma_{S,\mathrm{Born}} = 1$, $\Gamma_{P,\mathrm{Born}} = \gamma_5$, and $\Gamma_{A,\mathrm{Born}} = \gamma_4\gamma_5$.

The renormalization constant of the axial vector current can be directly determined from the axial Ward identity

$$Z_A = \frac{2m_q \langle P(t) P(0) \rangle}{\langle \partial_4 A_4(t) P(0) \rangle}. \tag{40}$$

The wave function renormalization constant Z_q can thus be obtained from Λ_A and Z_A, $Z_q(\mu) = Z_A \Lambda_A$. In Fig. 14 we plot Z_A. We find that the right-hand side of (40) is independent of t, except for the points close to source and sink, as expected. We extrapolate Z_A linearly in am_q to the chiral limit, as shown in Fig. 15. The final results are given in Table VIII. The corresponding fully tadpole improved (FTI) perturbative numbers [19] are $Z_A = 1.358$ at $\beta = 8.0$ and $Z_A = 1.303$ at $\beta = 8.45$. They lie 15%–8% below their nonperturbative values.

Note that the renormalization constants depend strongly on the choice of gauge field action [19]. This is confirmed by nonperturbative studies. The Iwasaki action appears to give a noticeably larger value for Z_A [36], albeit on coarser lattices, while the value of the plaquette action lies significantly below one at comparable couplings [37].

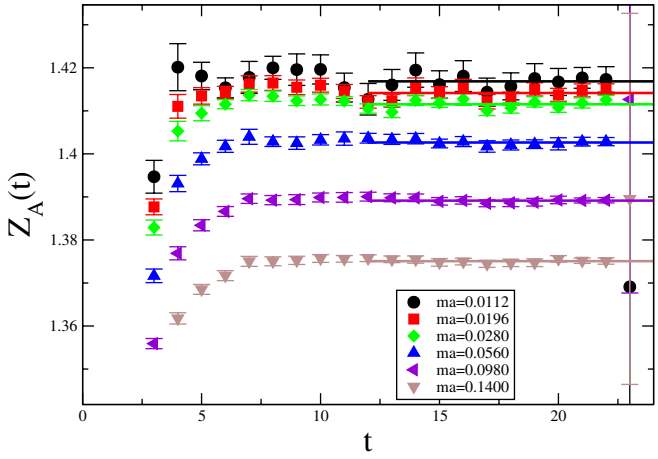

FIG. 14 (color online). The renormalization constant Z_A on the $24^3 48$ lattice at $\beta = 8.45$.

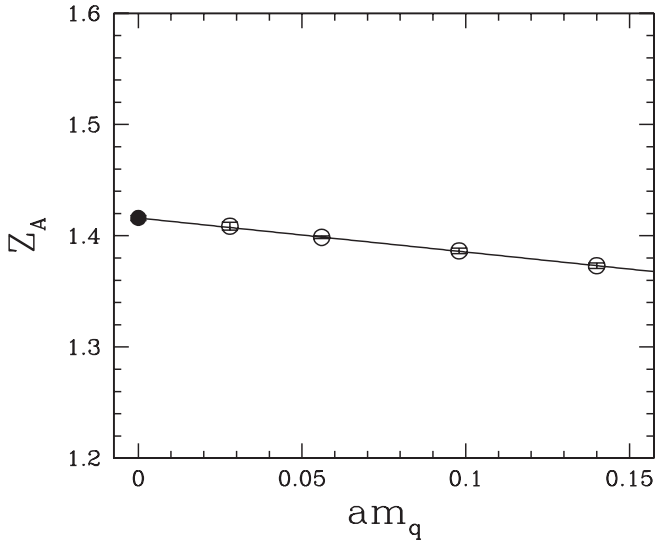

FIG. 15. Chiral extrapolation of Z_A on the $24^3 48$ lattice at $\beta = 8.45$, together with its value in the chiral limit (●).

Let us now turn to the calculation of $\Lambda_S(p)$, $\Lambda_P(p)$, and $\Lambda_A(p)$. We denote the expressions at finite m_q by $\Lambda(p, m_q)$. Strictly speaking, $\Lambda_S(p, m_q)$ and $\Lambda_P(p, m_q)$ cannot be

TABLE VIII. The renormalization constant of the axial vector and the scalar current.

β	V	Z_A	Z_S^{RGI}
8.0	$16^3 32$	1.59(1)	1.18(2)
8.45	$16^3 32$	1.41(1)	1.02(1)
8.45	$24^3 48$	1.42(1)	···

extrapolated to the chiral limit. Because of the zero modes, both $\Lambda_S(p, m_q)$ and $\Lambda_P(p, m_q)$ diverge $\propto 1/m_q^2$. This is an artefact of the quenched approximation. On top of that, $\Lambda_P(p, m_q)$ receives a contribution $\propto \Sigma/(m_q p^2)$. This term is due to spontaneous chiral symmetry breaking [35,38]. We thus expect the following dependence on the quark mass:

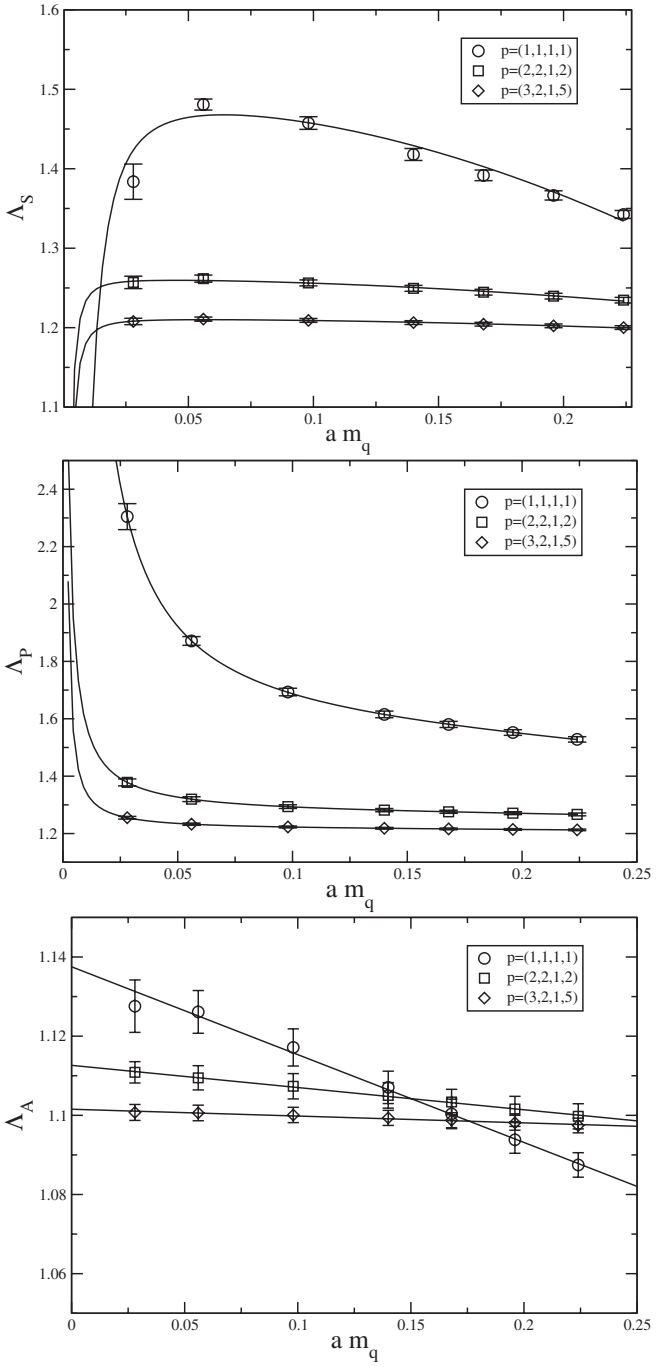

FIG. 16. Chiral extrapolation of Λ_S (top panel), Λ_P (middle panel), and Λ_A (bottom panel) on the $16^3 32$ lattice at $\beta = 8.45$ for some representative momenta $p = (n_1, n_2, n_3, n_4)$ in units of $2\pi/aL$ (n_1, n_2, n_3) and π/aL (n_4).

$$\Lambda_S(p, m_q) = \frac{C_1^S(p)}{(am_q)^2} + C_3^S(p) + C_4^S(p) am_q, \tag{41}$$

$$\Lambda_P(p, m_q) = \frac{C_1^P(p)}{(am_q)^2} + \frac{C_2^P(p)}{am_q} + C_3^P(p) + C_4^P(p) am_q, \tag{42}$$

$$\Lambda_A(p, m_q) = C_3^A(p) + C_4^A(p) am_q, \tag{43}$$

neglecting terms of $O(m_q^2)$. This behavior is indeed shown by the data. In Fig. 16 we plot $\Lambda_S(p, m_q)$, $\Lambda_P(p, m_q)$, and $\Lambda_A(p, m_q)$ for three different momenta, together with a fit of (41)–(43) to the data. We identify $\Lambda_S(p)$, $\Lambda_P(p)$, and $\Lambda_A(p)$ with $C_3^S(p)$, $C_3^P(p)$, and $C_3^A(p)$, respectively, from which we derive

$$Z_S(\mu) = \frac{\Lambda_A(\mu)}{\Lambda_S(\mu)} Z_A, \qquad Z_P(\mu) = \frac{\Lambda_A(\mu)}{\Lambda_P(\mu)} Z_A. \tag{44}$$

We expect $Z_S(\mu) = Z_P(\mu)$ due to chiral symmetry. To test this relation, we plot the ratio Λ_S/Λ_P in Fig. 17. We find good agreement between Z_S and Z_P for all momenta. In the following we shall make use of a combined fit of $\Lambda_S(p, m_q)$ and $\Lambda_P(p, m_q)$, in which we set $C_3^S(p) = C_3^P(p)$.

We are finally interested in Z_S in the $\overline{\text{MS}}$ scheme at a given scale μ. To convert our numbers from the RI′-MOM scheme, in which we were working so far, to the $\overline{\text{MS}}$ scheme, we proceed in two steps. In the first step we match to the scale invariant RGI scheme,

$$Z_S^{\text{RGI}} = \Delta^{\text{RI}'\text{-MOM}}(\mu) Z_S(\mu), \tag{45}$$

and in the second step we evolve Z_S^{RGI} to the targeted scale in the $\overline{\text{MS}}$ scheme,

$$Z_S^{\overline{\text{MS}}}(\mu) = \Delta^{\overline{\text{MS}}}(\mu)^{-1} Z_S^{\text{RGI}}. \tag{46}$$

The matching coefficients $\Delta^{\text{RI}'\text{-MOM}}(\mu)$ and $\Delta^{\overline{\text{MS}}}(\mu)$ are

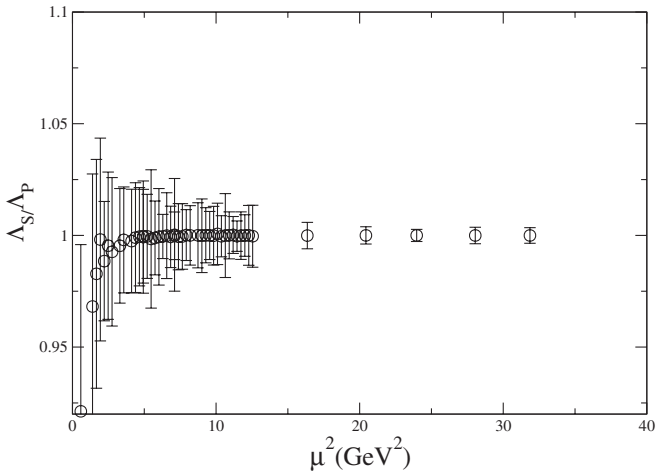

FIG. 17. The ratio $\Lambda_S(\mu)/\Lambda_P(\mu)$ as a function of μ on the $16^3 32$ lattice at $\beta = 8.45$.

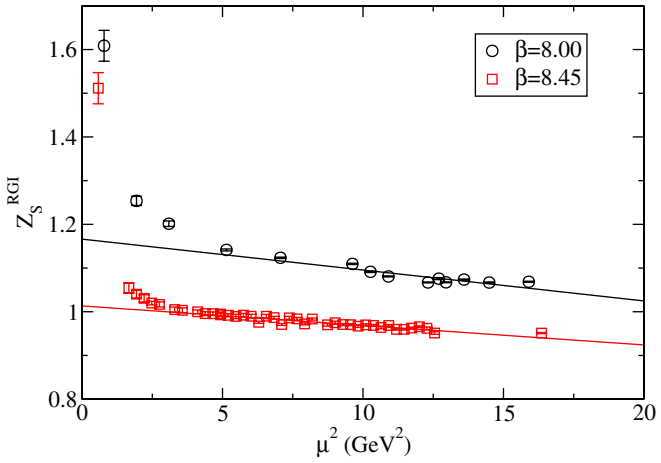

FIG. 18 (color online). The scale invariant renormalization constant Z_S^{RGI} on the $16^3 32$ lattice at $\beta = 8.0$ (○) and $\beta = 8.45$ (□).

known perturbatively to four loops [39]. In Fig. 18 we show Z_S^{RGI}. The result is not quite independent of the scale parameter μ as it should be, but shows a linear decrease in μ^2 for $\mu \gtrsim 2$ GeV. We attribute this behavior to lattice artefacts of $O(a^2\mu^2)$. Indeed, the slope of Z_S^{RGI} at our two different β values scales like a^2 to a good approximation. We thus fit the lattice result by

$$Z_S^{\mathrm{RGI,LAT}} = C_0 + C_1(a\mu)^2 \tag{47}$$

and identify the physical value of Z_S^{RGI} with C_0. The results are given in Table VIII. The four-loop value for $\Delta_S^{\overline{\mathrm{MS}}}(\mu)$ has been given in [40]. At $\mu = 2$ GeV it is $\Delta_S^{\overline{\mathrm{MS}}}(2\ \mathrm{GeV}) = 0.721(10)$. The error is a reflection of the error of $\Lambda^{\overline{\mathrm{MS}}}$. The nonperturbative result at $\beta = 8.45$ is in good agreement with $Z_S^{\mathrm{FTI,RGI}}$ from [19].

VI. CHIRAL CONDENSATE AND QUARK MASSES

Having determined the renormalization constant of the scalar density, we may now compute the renormalized chiral condensate and light and strange quark masses.

TABLE IX. The chiral condensate.

β	V	$\langle\bar\psi\psi\rangle^{\overline{\mathrm{MS}}}(2\ \mathrm{GeV})$
8.0	$16^3 32$	$-[324(8)\ \mathrm{MeV}]^3$
8.45	$24^3 48$	$-[296(11)\ \mathrm{MeV}]^3$

Let us first consider the chiral condensate $\langle\bar\psi\psi\rangle$. Strictly speaking, $\langle\bar\psi\psi\rangle$ is not defined in the quenched theory due to the presence of a logarithmic singularity in the chiral limit. Nevertheless, we may identify $-\langle\bar\psi\psi\rangle$ with Σ and assume that Σ renormalizes like (the finite part of) the scalar density. In the $\overline{\mathrm{MS}}$ scheme at $\mu = 2$ GeV we then have

$$\langle\bar\psi\psi\rangle^{\overline{\mathrm{MS}}}(2\ \mathrm{GeV}) = -Z_S^{\overline{\mathrm{MS}}}(2\ \mathrm{GeV})\Sigma. \tag{48}$$

Taking Σ from our second fit in Table V, where we have fixed δ to its theoretical value 0.183, this leads to the results in Table IX. The lower number at the larger β value is in reasonable agreement with phenomenology and other quenched lattice calculations [41]. A better way to determine Σ is by means of the spectral density [42,43], which we will address in a separate publication [44].

Let us now turn to the evaluation of the quark masses. We shall assume (26) with $\alpha_\Phi^q = 0$ as the basic functional form for the relation between the quark masses and the pseudoscalar mass:

$$m_{\mathrm{PS}}^2 = Xm_q + Ym_q \ln m_q + Zm_q^2. \tag{49}$$

For nondegenerate quark masses, m_q^a and m_q^b, chiral perturbation theory gives the result

$$(m_{\mathrm{PS}}^{ab})^2 = X\left(\frac{m_q^a + m_q^b}{2}\right) + Y\left(\frac{m_q^a + m_q^b}{2}\right) \times \left(\frac{m_q^a \ln m_q^a - m_q^b \ln m_q^b}{m_q^a - m_q^b} - 1\right) + Z\left(\frac{m_q^a + m_q^b}{2}\right)^2 \tag{50}$$

with no new parameter. In fact, (50) reduces exactly to (49) in the limit $m_q^a \to m_q^b$. We fit (49) to our data to determine the coefficients X, Y, and Z. The light quark mass, $m_\ell = (m_u + m_d)/2$, is then found from

$$m_{\pi^+}^2 = Xm_\ell + Ym_\ell \ln m_\ell + Zm_\ell^2, \tag{51}$$

while we compute the strange quark mass from

$$\frac{m_{K^+}^2 + m_{K^0}^2}{2} = X\left(\frac{m_\ell + m_s}{2}\right) + Y\left(\frac{m_\ell + m_s}{2}\right) \times \left(\frac{m_\ell \ln m_\ell - m_s \ln m_s}{m_\ell - m_s} - 1\right) + Z\left(\frac{m_\ell + m_s}{2}\right)^2. \tag{52}$$

The results are given in Table X. The renormalized quark masses are obtained from

TABLE X. The unrenormalized and renormalized quark masses.

β	V	m_ℓ (MeV)	m_s (MeV)	$m_\ell^{\overline{\mathrm{MS}}}(2\ \mathrm{GeV})$ (MeV)	$m_s^{\overline{\mathrm{MS}}}(2\ \mathrm{GeV})$ (MeV)
8.0	$16^3 32$	6.3(1)	203(4)	3.8(1)	124(3)
8.45	$24^3 48$	5.3(3)	160(5)	3.8(2)	114(4)

$$m_q^R = Z_m m_q \tag{53}$$

and $Z_S = 1/Z_m$ given in Table VIII. In Table X we state the final results in the $\overline{\text{MS}}$ scheme at $\mu = 2$ GeV. Our findings are in good agreement with other nonperturbative calculations of the quark masses in the quenched approximation [4,5,40,45].

VII. CONCLUSIONS

The extrapolation to the chiral limit has been a major challenge in lattice QCD. We have shown that with using overlap fermions it is possible to progress to small quark masses. Here we have simulated pion masses down to $m_\pi \approx 250$ MeV on both of our lattices. We have made an attempt to compute the low-energy constants of quenched chiral perturbation theory, with some success. Our results turn out to be consistent with the predicted and/or phenomenological values. To fully exploit the potential of overlap fermions at small quark masses, one will, however, need a statistics of several thousand independent gauge field configurations.

The pion mass was found to depend on the topological charge $|Q|$ at small quark masses. No such behavior was found for the pseudoscalar decay constant, but a similar effect is expected to show up in the chiral condensate [42].

Overlap fermions, in combination with the Lüscher-Weisz gauge field action, show good scaling properties already at lattice spacing $a \approx 0.15$ fm, owing to the fact that they are automatically $O(a)$ improved, on shell and off shell. This helps to reduce the large numerical overhead in the algorithm.

The calculations performed in this paper test many of the ingredients needed for a simulation of full QCD, and thus provide a lesson for future applications.

ACKNOWLEDGMENTS

The numerical calculations have been performed on the IBM p690 at HLRN (Berlin) and NIC (Jülich), as well as on the PC farm at DESY (Zeuthen). Furthermore, we made use of the facilities on the CCHPCF at Cambridge and of HPCx, the UK's national high performance computing service, which is provided by EPCC at the University of Edinburgh and by CCLRC Daresbury Laboratory, and funded by the Office of Science and Technology through EPSRC's High End Computing Program. We thank all institutions. This work has been supported in part by the EU Integrated Infrastructure Initiative Hadron Physics (I3HP) under Contract No. RII3-CT-2004-506078 and by the DFG under Contract No. FOR 465 (Forschergruppe Gitter-Hadronen-Phänomenologie). T. S. is supported by the Alexander von Humboldt Foundation.

[1] H. Neuberger, Phys. Lett. B **417**, 141 (1998); **427**, 353 (1998).
[2] M. Lüscher, Phys. Lett. B **428**, 342 (1998).
[3] S. Capitani, M. Göckeler, R. Horsley, P. E. L. Rakow, and G. Schierholz, Phys. Lett. B **468**, 150 (1999).
[4] L. Giusti, C. Hoelbling, and C. Rebbi, Phys. Rev. D **64**, 114508 (2001); **65**, 079903(E) (2002); N. Garron, L. Giusti, C. Hoelbling, L. Lellouch, and C. Rebbi, Phys. Rev. Lett. **92**, 042001 (2004); F. Berruto, N. Garron, C. Hoelbling, J. Howard, L. Lellouch, S. Necco, C. Rebbi, and N. Shoresh, Nucl. Phys. B, Proc. Suppl. **140**, 264 (2005).
[5] S. J. Dong, F. X. Lee, K. F. Liu, and J. B. Zhang, Phys. Rev. Lett. **85**, 5051 (2000); S. J. Dong, T. Draper, I. Horvath, F. X. Lee, K. F. Liu, and J. B. Zhang, Phys. Rev. D **65**, 054507 (2002); F. X. Lee, S. J. Dong, T. Draper, I. Horvath, K. F. Liu, N. Mathur, and J. B. Zhang, Nucl. Phys. B, Proc. Suppl. **119**, 296 (2003); N. Mathur, F. X. Lee, A. Alexandru, C. Bennhold, Y. Chen, S. J. Dong, T. Draper, I. Horvath, K. F. Liu, S. Tamhankar, and J. B. Zhang, Phys. Rev. D **70**, 074508 (2004).
[6] D. Galletly, M. Gürtler, R. Horsley, B. Joó, A. D. Kennedy, H. Perlt, B. J. Pendleton, P. E. L. Rakow, G. Schierholz, A. Schiller, and T. Streuer, Nucl. Phys. B, Proc. Suppl. **129**, 453 (2004).
[7] W. Bietenholz, T. Chiarappa, K. Jansen, K. I. Nagai, and S. Shcheredin, J. High Energy Phys. 02 (2004) 023.
[8] P. Hernandez, K. Jansen, and M. Lüscher, Nucl. Phys. **B552**, 363 (1999).
[9] G. Colangelo, Nucl. Phys. B, Proc. Suppl. **140**, 120 (2005).
[10] D. Galletly, M. Gürtler, R. Horsley, K. Koller, V. Linke, P. E. L. Rakow, C. J. Roberts, G. Schierholz, and T. Streuer, Proc. Sci., LAT2005 (2005) 363 [hep-lat/0510050].
[11] M. Gürtler, R. Horsley, V. Linke, H. Perlt, P. E. L. Rakow, G. Schierholz, A. Schiller, and T. Streuer, Nucl. Phys. B, Proc. Suppl. **140**, 707 (2005).
[12] E.-M. Ilgenfritz, K. Koller, Y. Koma, G. Schierholz, T. Streuer, and V. Weinberg, Nucl. Phys. B, Proc. Suppl. **153**, 328 (2006).
[13] V. Weinberg, E.-M. Ilgenfritz, K. Koller, Y. Koma, G. Schierholz, and T. Streuer, Proc. Sci., LAT2005 (2005) 171 [hep-lat/0510056].
[14] L. Giusti, C. Hoelbling, M. Lüscher, and H. Wittig, Comput. Phys. Commun. **153**, 31 (2003).
[15] M. Lüscher and P. Weisz, Commun. Math. Phys. **97**, 59 (1985).
[16] C. Gattringer, R. Hoffmann, and S. Schaefer, Phys. Rev. D **65**, 094503 (2002).

[17] K. Symanzik, Nucl. Phys. **B226**, 187 (1983).
[18] M. Göckeler, A. S. Kronfeld, M. L. Laursen, G. Schierholz, and U.-J. Wiese, Phys. Lett. B **233**, 192 (1989).
[19] R. Horsley, H. Perlt, P. E. L. Rakow, G. Schierholz, and A. Schiller, Nucl. Phys. **B693**, 3 (2004); **B713**, 601(E) (2005).
[20] M. Göckeler, R. Horsley, E.-M. Ilgenfritz, H. Perlt, P. Rakow, G. Schierholz, and A. Schiller, Phys. Rev. D **53**, 2317 (1996).
[21] T. DeGrand and S. Schaefer, Comput. Phys. Commun. **159**, 185 (2004); L. Giusti, P. Hernandez, M. Laine, P. Weisz, and H. Wittig, J. High Energy Phys. 04 (2004) 013; A. O'Cais, K. J. Juge, M. J. Peardon, S. M. Ryan, and J. I. Skullerud, Nucl. Phys. B, Proc. Suppl. **140**, 844 (2005).
[22] G. P. Lepage, Report No. CLNS-89-971.
[23] M. Göckeler, R. Horsley, H. Perlt, P. Rakow, G. Schierholz, A. Schiller, and P. Stephenson, Phys. Rev. D **57**, 5562 (1998).
[24] G. Colangelo and E. Pallante, Nucl. Phys. **B520**, 433 (1998).
[25] C. W. Bernard and M. F. L. Golterman, Phys. Rev. D **46**, 853 (1992).
[26] S. R. Sharpe, Phys. Rev. D **46**, 3146 (1992).
[27] J. Gasser and H. Leutwyler, Nucl. Phys. **B250**, 465 (1985).
[28] J. Bijnens, AIP Conf. Proc. **768**, 153 (2005).
[29] J. Heitger, R. Sommer, and H. Wittig, Nucl. Phys. **B588**, 377 (2000).
[30] E. Witten, Nucl. Phys. **B156**, 269 (1979); G. Veneziano, Nucl. Phys. **B159**, 213 (1979).
[31] R. Brower, S. Chandrasekharan, J. W. Negele, and U.-J. Wiese, Phys. Lett. B **560**, 64 (2003).
[32] M. Booth, G. Chiladze, and A. F. Falk, Phys. Rev. D **55**, 3092 (1997).
[33] J. N. Labrenz and S. R. Sharpe, Phys. Rev. D **54**, 4595 (1996).
[34] G. Martinelli, C. Pittori, C. T. Sachrajda, M. Testa, and A. Vladikas, Nucl. Phys. **B445**, 81 (1995).
[35] M. Göckeler, R. Horsley, H. Oelrich, H. Perlt, D. Petters, P. E. L. Rakow, A. Schäfer, G. Schierholz, and A. Schiller, Nucl. Phys. **B544**, 699 (1999).
[36] J. B. Zhang, N. Mathur, S. J. Dong, T. Draper, I. Horvath, F. X. Lee, D. B. Leinweber, K. F. Liu, and A. G. Williams, Phys. Rev. D **72**, 114509 (2005).
[37] T. Blum, N. Christ, C. Cristian, C. Dawson, G. Fleming, G. Liu, R. Mawhinney, A. Soni, P. Vranas, M. Wingate, L. Wu, and Y. Zhestkov, Phys. Rev. D **66**, 014504 (2002).
[38] H. Pagels, Phys. Rev. D **19**, 3080 (1979).
[39] K. G. Chetyrkin, Phys. Lett. B **404**, 161 (1997); J. A. M. Vermaseren, S. A. Larin, and T. van Ritbergen, Phys. Lett. B **405**, 327 (1997); K. G. Chetyrkin and A. Rétey, Nucl. Phys. **B583**, 3 (2000); see also M. Göckeler, R. Horsley, A. C. Irving, D. Pleiter, P. E. L. Rakow, G. Schierholz, H. Stüben, and J. M. Zanotti, Phys. Rev. D **73**, 054508 (2006).
[40] M. Göckeler, R. Horsley, H. Oelrich, D. Petters, D. Pleiter, P. E. L. Rakow, G. Schierholz, and P. Stephenson, Phys. Rev. D **62**, 054504 (2000).
[41] L. Giusti, F. Rapuano, M. Talevi, and A. Vladikas, Nucl. Phys. **B538**, 249 (1999); T. A. DeGrand, Phys. Rev. D **64**, 117501 (2001); P. Hernandez, K. Jansen, L. Lellouch, and H. Wittig, J. High Energy Phys. 07 (2001) 018; L. Giusti, C. Hoelbling, and C. Rebbi, Phys. Rev. D **64**, 114508 (2001); **65**, 079903(E) (2002); T. Blum, P. Chen, N. Christ, C. Cristian, C. Dawson, G. Fleming, A. Kaehler, X. Liao, G. Liu, C. Malureanu, R. Mawhinney, S. Ohta, G. Siegert, A. Soni, C. Sui, P. Vranas, M. Wingate, L. Wu, and Y. Zhestkov, Phys. Rev. D **69**, 074502 (2004); D. Bećirević and V. Lubicz, Phys. Lett. B **600**, 83 (2004); V. Gimenez, V. Lubicz, F. Mescia, V. Porretti, and J. Reyes, Eur. Phys. J. C **41**, 535 (2005); C. Gattringer, P. Huber, and C. B. Lang, Phys. Rev. D **72**, 094510 (2005).
[42] J. C. Osborn, D. Toublan, and J. J. M. Verbaarschot, Nucl. Phys. **B540**, 317 (1999).
[43] P. H. Damgaard, Nucl. Phys. **B608**, 162 (2001).
[44] M. Gürtler *et al.* (unpublished).
[45] J. Garden, J. Heitger, R. Sommer, and H. Wittig, Nucl. Phys. **B571**, 237 (2000).